

Spectroscopic Investigation of Cr(III)- and Cr(VI)-Treated Nanoscale Zerovalent Iron

BRUCE A. MANNING,^{*,†} JON R. KISER,[†]
 HANCHEOL KWON,[‡] AND
 SUSHIL RAJ KANEL[§]

*Department of Chemistry and Biochemistry,
 San Francisco State University, 1600 Holloway Avenue,
 San Francisco, California 94132, Department of Chemistry,
 University of Illinois, Urbana-Champaign, Chemical and Life
 Sciences Lab A514 CLSL BOX 38-6, 600 South Mathews
 Avenue, Urbana, Illinois 61801, Department of Environmental
 Science and Engineering, Gwangju Institute of Science and
 Technology (GIST), 1 Oryong-dong,
 Buk-gu, Gwangju 500-712, Korea*

The reaction of hexavalent chromium (Cr(VI)) with zerovalent iron (Fe⁰) during soil and groundwater remediation is an important environmental process. This study used several techniques including X-ray photoelectron spectroscopy (XPS) and X-ray absorption spectroscopy to investigate nanometer scale Fe⁰ particles (nano Fe⁰) treated with Cr(III) and Cr(VI). X-ray diffraction and XPS analyses of oxidized nano Fe⁰ showed the crystalline Fe(III) phase is composed of lepidocrocite (γ -FeOOH). Results of XPS Cr 2p data and Cr K-edge X-ray absorption near edge spectroscopy (XANES) provided evidence that Cr(VI) was entirely reduced to Cr(III) by nano Fe⁰ with no residual Cr(VI) after reaction. In addition, XPS and XANES results of Cr(III) precipitated as Cr(OH)₃ in the presence of corroding nano Fe⁰ were nearly identical to the Cr(VI)-nano Fe⁰ reaction product. Detailed analysis of XPS O 1s line spectra revealed that both Cr(III)- and Cr(VI)-treated nano Fe⁰ yielded a predominantly hydroxylated Cr(OH)₃ and/or a mixed phase Cr_xFe_{1-x}(OH)₃ product. The structure of the Cr(III)- and Cr(VI)-treated nano Fe⁰ determined using extended X-ray absorption fine structure spectroscopy (EXAFS) revealed octahedral Cr(III) with Cr–O interatomic distances between 1.97 and 1.98 Å for both Cr(III) and Cr(VI) treatments and a pronounced Cr–Cr second interatomic shell at 3.01 Å. Our results suggest that the reaction product of Cr(VI)-treated nano Fe⁰ is either a poorly ordered Cr(OH)₃ precipitate or possibly a mixed phase Cr_xFe_{1-x}(OH)₃ product, both of which are highly insoluble under environmental conditions.

Introduction

Chromium(VI) is an industrial contaminant in soil and groundwater and is a known human carcinogen of concern (1, 2). Remediation of Cr(VI) using permeable reactive barriers containing zerovalent iron (Fe⁰) has been extensively inves-

tigated and has been shown to effectively immobilize Cr(VI) (3–10). Zerovalent iron is an efficient in-situ remediation material due to its ability to facilitate chemical reduction and form high surface area Fe⁰ corrosion products such as Fe(III) hydroxides and oxyhydroxides which immobilize pollutants (11–14). The Cr(VI) removal mechanism involves reduction of dissolved chromate (CrO₄²⁻) to insoluble Cr(III) followed by precipitation of Cr(OH)₃ or coprecipitation of Cr(III) with Fe(III) oxides/hydroxides (4, 5, 15–17). In addition to reduction by Fe⁰, it is well-established that Fe(II), an intermediate in the Fe⁰ corrosion reaction, is an effective reducing agent for Cr(VI) (18–22).

Recent investigations of synthetic Fe⁰ nanoparticles have shown that this material is effective in remediation of chlorinated organic compounds (TCE and PCBs) (23–25), As(III) (26), Pb(II), and Cr(VI) (17, 27). Ponder et al. (17) investigated the kinetics of Cr(VI) reduction by both unsupported nano Fe⁰ and resin-supported nano Fe⁰ ("Ferragel") and concluded that the Cr(VI) reduction rate was up to 30 times greater than conventional Fe⁰ filings. The mechanisms of Cr(VI) reduction by both Fe⁰ nanoparticles and Fe⁰ filings are similar. Both involve complex surface chemistry during in-situ corrosion of the Fe⁰ surface, reduction of Cr(VI) to Cr(III) through coupled oxidation of Fe⁰ and Fe²⁺, and coprecipitation of Cr(III) with Fe(III) in a poorly defined Cr(III)/Fe(III) mixed hydroxide phase (8, 17, 27). Another complicating factor uncovered during electrochemical investigations of Cr(VI) reduction by Fe⁰ wire involves surface passivation of the corroding Fe⁰ surface where absolute, first-order Cr(VI) removal rates decrease with increasing Cr(VI) concentration (8). This phenomenon has also been reported for Cr(VI) reduction by the Fe²⁺-bearing mineral magnetite (Fe₃O₄) (28) which is a corrosion product on Fe⁰ filing surfaces (14).

Though several studies have investigated Cr(VI) reduction by various Fe⁰ materials the identity of the solid-phase reaction product remains inconclusive. Several investigations have proposed formation of a mixed Fe(III)–Cr(III) hydroxide solid (7, 15, 17) according to the following reaction:



The Cr(III)–Fe(III) mixed phase may contain between 25% ($x = 0.25$) and 67% Cr(III) depending on reaction conditions such as pH and Cr(III) concentration (15, 17). Reaction (1) has also been reported in natural groundwater systems where Cr(VI) is reduced to Cr(III) by Fe(II) (18, 29). A Cr(III)-containing Cr₂O₃-like phase was reported in association with Fe⁰ filing corrosion products based on X-ray photoelectron spectroscopy (XPS) (4) and backscattered electron imaging (5). In addition, zones of Cr(OH)₃ have been reported to form in association with Fe(III) oxyhydroxide (FeOOH) after reaction of Cr(VI) with mm-scale Fe⁰ chips (5). Investigation of Cr(III) adsorption on hydrous ferric oxide (HFO) and goethite (α -FeOOH) using extended X-ray absorption fine structure (EXAFS) spectroscopy (30) found differences in the local structure of Cr(III) depending on whether Cr(III) was added alone or as a binary Cr(III)–Fe(III) system. The most favorable models were a Cr(III) oxyhydroxide (γ -CrOOH) polymer in the single Cr(III) ion system and a Cr(III)-substituted α -(Fe, Cr)OOH framework in the binary system (30). In addition, formation of the α -CrOOH polymorph was reported after reduction of Cr(VI) by magnetite (28). Though it is possible that CrOOH exists on intact HFO surfaces, it has not yet been reported in association with Fe⁰ corrosion products.

* Corresponding author: phone: 415-338-1292; fax: 415-338-2384; e-mail: bmannings@sfsu.edu.

† San Francisco State University.

‡ University of Illinois.

§ Gwangju Institute of Science and Technology.

In this paper we investigate Cr(III)- and Cr(VI)-treated synthetic nano Fe⁰ using X-ray spectroscopic techniques to help shed light on the structure and identity of the Cr and Fe reaction products. The objectives are to (1) analyze the electronic structure of Cr, Fe, and O in Cr(III)- and Cr(VI)-treated nano Fe⁰ using XPS, (2) examine the electronic structure of Cr in Cr(III)- and Cr(VI)-treated nano Fe⁰ using K-edge X-ray absorption near edge spectroscopy (XANES), and (3) investigate the local atomic structural environment of Cr in Cr(III)- and Cr(VI)-treated nano Fe⁰ using EXAFS spectroscopy.

Experimental Section

Materials. The reagents used in this study (FeCl₂, CrCl₃, Na₂CrO₄, HCl, NaOH, and NaBH₄) were reagent grade and deionized (DI) water as used in all preparations. A 100 mesh electrolytic Fe⁰ powder (Fisher) was used as a reference material without further preparation. Nano Fe⁰ particles were prepared using a method similar to Ponder et al. (17, 27) by reacting 500 mL of Ar-purged 0.012 M FeCl₂ (in 30% ethanol) with 8–10 mL of 0.53 M NaBH₄ in an Ar-purged flask while stirring. This method used a Fe:B molar ratio = 0.4 and typically yielded 0.334 g nano Fe⁰ per batch. The synthesized nano Fe⁰ particles were recovered by rinsing the solid three times with Ar-purged 30% ethanol to remove unreacted reagent and vacuum removal of overlying solutions. Samples of nano Fe⁰ particles were either stored in an Ar-purged desiccator or immediately subjected to batch reactions as described below. In addition, a synthetic lepidocrocite (γ -FeOOH) sample was prepared using a previously described method (31).

Nano Fe⁰ Particle Characterization. Unreacted nano Fe⁰ particles were characterized by transmission electron microscopy (TEM) using a Philips CM 300 with an accelerated voltage of 300 keV. The TEM samples were prepared by dropping nano Fe⁰ suspension on a carbon-coated copper grid and drying in vacuum oven at 60 °C. The specific surface area of nano Fe⁰ was measured by the BET N₂ method at 77 K using a Micromeritics ASAP 2010 automatic analyzer. The measured nano Fe⁰ surface area was 24.4 m² g⁻¹. Unreacted nano Fe⁰ and nano Fe⁰ corroded in 1.0 mM NaCl were analyzed by X-ray diffraction (XRD) with a Bruker D8 ADVANCE X-ray diffractometer set at 0.04 degrees/step angle resolution using Bragg–Brentano primary beam optics, 0.6 mm detector slit, graphite monochromator, and NaI scintillation detector.

Cr(VI) and Cr(III) Treatments. Preparation of samples for XPS and EXAFS analyses involved using batches of 0.334 g nano Fe⁰ (6.0 × 10⁻³ mol Fe) reacted with 500 mL of Ar-purged 0.20 mM Cr(III) or Cr(VI) in 1.0 mM NaCl for 72 h. The pH of the reaction mixture was initially adjusted to 7.0 and became alkaline (pH 8.2) during the reaction. After 72 h, the reacted Fe⁰ particles were allowed to settle and 20 mL aliquots of the overlying solution were filtered (0.1 μm). Total dissolved Cr was analyzed by flame atomic absorption spectrometry (FAAS) with a Varian 220 FS AAS. The reacted particles were rinsed twice with Ar-purged 30% ethanol and stored in an Ar-purged desiccator for XPS and EXAFS analyses. Samples of corroded 100 mesh Fe⁰ powder and nano Fe⁰ (without Cr(III) or Cr(VI)) were prepared by mixing 0.334 g solid in 100 mL of 1.0 mM NaCl for 72 followed by preservation in Ar.

XPS Analysis. X-ray photoelectron spectroscopy was performed with a Physical Electronics PHI5400 X-ray photoelectron spectrometer. The XPS unit used a Mg K α X-ray source (20 mA and 15 kV) and was equipped with a UHV chamber operating below 1 × 10⁻⁸ Torr. The X-ray beam was incident normal to the sample and the hemispherical detector was oriented at 45° to the sample stage. Samples of unreacted nano Fe⁰, corroded nano Fe⁰, Cr(III)/Cr(VI)-treated nano Fe⁰,

and synthetic lepidocrocite (γ -FeOOH) were dried under Ar (95 °C for 24 h) and mounted on double-sided Cu tape. High-resolution C 1s, O 1s, Cr 2p, and Fe 2p line scans involved collection of 80 sweeps per element at 0.1 eV/step energy resolution. Experimental O 1s, Fe 2p, and Cr 2p binding energies (BEs) were corrected for surface charging by comparison of experimental C 1s main peak centroids to the theoretical C 1s line energy of 285.0 eV (32, 33). The C 1s line is the result of trace contamination of the sample surface with adventitious hydrocarbon (32, 33). Energy differences between theoretical and measured C 1s lines were generally less than ±4 eV. Binding energies and XPS peak assignments were made on C 1s corrected data with Gaussian–Lorentzian curve fitting using AugerScan 3.0 software.

X-ray Absorption Spectroscopy. Samples of nano Fe⁰, Cr(III)/Cr(VI)-treated nano Fe⁰, and several model compounds (Cr⁰ and Fe⁰ metal, Cr and Fe salts, FeO, γ -FeOOH, and Cr₂O₃) were analyzed on GeoSoilEnviroCARS beamline 13 BM–D at Argonne National Laboratory's Advanced Photon Source (APS). Sample preparation was performed as described above within 7 days of analysis but samples were maintained as hydrated pastes in Ar-purged bottles. Samples were held between kapton tape in slotted 2 mm-thick plexiglass plates and mounted in the X-ray beam at a 45° angle. The K-edge XANES scans for Cr (5864–6051 eV) and Fe (6982–7212 eV) were recorded with step increments of 0.5 eV controlled with a Si(111) monochromator. Energy calibration was performed by assigning the K-edge energy of 7111.0 eV to Fe⁰ foil. X-ray fluorescence was recorded using a 16 element Ge solid-state array multi-element detector (Canberra) and the incident beam intensity (I_0) was recorded using a standard ionization detector. Extended scans were collected with 2 eV steps to 6370 eV for Cr for EXAFS analyses (eight scans per sample).

Analysis of EXAFS and XANES data was performed using SixPACK software (34) and IFEFFIT (35). The individual scans were averaged followed by linear preedge subtraction, linear background removal, unit step edge normalization, isolation of the $\chi(k)$ function with a cubic spline function, followed by k^3 weighting. Theoretical EXAFS amplitude and phase functions for Cr–O, Cr–Cr, and Cr–Fe single scattering paths were then generated by FEFF 7.0 (36). Fitted parameters such as amplitude reduction factor (S_0^2), Fermi shift (E_0), interatomic distance (R), and Debye–Waller factor (σ^2) were first established with reasonable guesses and were fitted in k -space. The Cr–O shell coordination number (N) was held constant at $N = 4$ for Cr(VI) and $N = 6$ for samples containing Cr(III). The S_0^2 value was established as 0.773 by fitting of a 2.0 mM Na₂CrO₄ solution EXAFS spectrum with fixed values of $N = 4$ O atoms and $R_{Cr-O} = 1.69 \text{ \AA}$ (37). Fitting of subsequent spectra used $S_0^2 = 0.773$ as a starting value which was only used as an adjustable parameter as the final step in the fit. In addition, the E_0 value was allowed to float by no more than ±10 eV and was internally linked for all interatomic shells in a given spectrum. Errors in the overall fits were determined using the following goodness of fit parameter:

$$\text{Fit}(\%) = \left(\frac{\sum (\chi_{\text{exp}} - \chi_{\text{fit}})^2}{\sum (\chi_{\text{exp}})^2} \right) \times 100$$

where χ_{exp} and χ_{fit} are the experimental and calculated $\chi(k)$ function data, respectively. Errors in individual parameters were established using SixPACK output and were ± 0.02 Å for R and ± 20% for N .

Results and Discussion

TEM and XRD Measurements. Figure 1 shows a TEM image of unreacted, synthetic nano Fe⁰. The material is composed of Fe⁰ particles in the 10–50 nm size range that are aggregated into chains and further linked into clusters of chains. These results appear similar to previous studies investigating nano

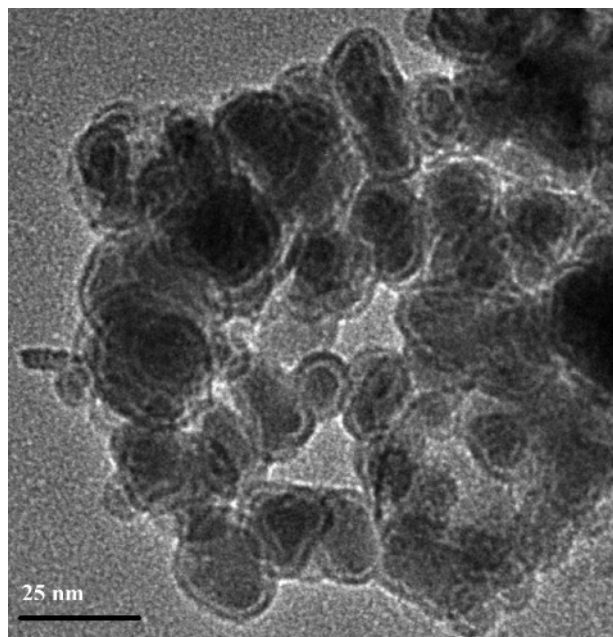


FIGURE 1. Transmission electron microscopy image of aggregated nano Fe⁰ particles. Scale bar = 25 nm.

Fe⁰ prepared by NaBH₄ reduction of Fe(II) (26, 38). The investigation by Nurmi et al. (38) used electron diffraction and found that synthetic nano Fe⁰ particles were composed of a core of either small crystallites of Fe⁰ or amorphous Fe⁰ covered with a polycrystalline Fe(III) oxide shell. Similarly, XPS analysis of our freshly prepared nano Fe⁰ (discussed below) revealed that surface Fe is in the Fe(III) oxidation state as an oxide or oxyhydroxide coating. Nano Fe⁰ reacted with 1.0 mM NaCl for 48 h followed by drying yielded a lepidocrocite (γ -FeOOH) corrosion product (see Figure S1 Supporting Information).

Cr(III) and Cr(VI) uptake by Nano Fe⁰. The Cr(III)- and Cr(VI)-treated nano Fe⁰ reaction proceeded rapidly and a noticeable orange corrosion product was visible within minutes of initiating the reaction. After 72 h the measured Cr(VI) and Cr(III) solid concentrations were 5.2 and 8.0 mmol g⁻¹ nano Fe⁰, respectively (Table 1), which corresponds to respective Cr:Fe mol:mol ratios of 0.29 and 0.45. This is comparable to previous studies of Cr(VI)-treated Fe⁰ where Cr:Fe mol:mol ratios between 0.7 and 1.6 were estimated (4). Despite the fact that nano Fe⁰ surface area was measured, we have avoided the use of surface coverage (mol·m⁻²) to express Cr content due to uncertainties in the surface area of the reaction product. Preliminary batch tests with Cr(III)

and Cr(VI) uptake by nano Fe⁰ suggest that this synthetic material is capable of producing Cr:Fe mol:mol ratios greater than one (data not shown). Our Cr:Fe mol:mol ratio estimates are in agreement with a generalized mechanism of Cr uptake postulated in earlier studies (4, 5, 17) where formation of a (Cr_{1-x}Fe_x)(OH)₃(s) phase where $x = 0.33$ was found (Cr:Fe mol:mol ratio = 2.03).

XPS Measurements. The C 1s line region was scanned and used to correct the absolute binding energy (BE) of subsequent scans for charging effects. The uncorrected C 1s line data for all samples (except Na₂CrO₄) gave a +3.4 eV shift from the theoretical C 1s line of 285.0 eV (32, 33) (Figure S2, Supporting Information). This shift was used to correct all subsequent Fe 2p, O 1s, and Cr 2p data analyses. High-resolution C 1s-corrected Fe 2p line region scans (Figure S3 Supporting Information) revealed that only Fe(III) was present on the surface of our Fe samples consistent with previous XPS work on nano Fe⁰ (17, 38), Fe⁰ filings (4, 7), and Fe⁰ foil (39). Under environmental conditions, the Fe(III) exists as a passivating layer on all Fe⁰ surfaces except those subject to extreme preparative measures such as cleaving and sputtering in a UHV environment (40). XANES analysis of unreacted nano Fe⁰ showed that the bulk of particles consisted of Fe⁰ (see Figure 4). Overall, the Fe 2p spectra (including the Fe 2p_{3/2} peak intensity) of unreacted nano Fe⁰ and 100 mesh Fe⁰ powder were nearly identical suggesting that the electronic state of surface Fe in synthetic nano Fe⁰ was comparable to the Fe oxide shell that forms on Fe⁰ metal powder exposed to air.

The XPS scans of the Cr 2p region are shown in Figure 2 with Cr 2p_{1/2} and Cr 2p_{3/2} lines at 587.2 and 577.7 eV, respectively. Measurement of the Cr 2p_{3/2} line binding energy of Na₂CrO₄ and CrCl₃ salts showed that the +3 formal oxidation state difference caused a shift of 1.8 eV in the spectrum. It can be readily seen that reduction of Cr(VI) to Cr(III) occurred during reaction with nano Fe⁰. The magnitude of the Cr 2p line spin-orbit splitting is 9.8 eV which is comparable to 9.7 eV splitting measured on Cr(VI)-treated Fe⁰ foil (39). Previous XPS investigation of the reaction of Cr(VI) with subsurface remediation material (Fe⁰ filing + quartz sand) gave Cr 2p line XPS spectra indicative of Cr₂O₃ (4) with the Cr 2p_{3/2} line peak split into a multiplet. We did not observe a Cr 2p_{3/2} line multiplet for either Cr(III)- or Cr(VI)-treated nano Fe⁰, but rather a single, smooth Gaussian-shaped peak indicative of Cr(OH)₃ (32). Quantitative curve fitting was applied to the Cr(III)- or Cr(VI)-treated nano Fe⁰ data (Figure 2) (see data in Table S1 in the Supporting Information). Both the Cr 2p_{1/2} and Cr 2p_{3/2} lines were described with one Gaussian shaped peak plus a contribution from a broad, higher energy peak and a low-intensity background. The fitted Cr 2p_{3/2} peak intensities of 19890 and

TABLE 1. Cr K-edge EXAFS Fitting Results for Model Systems (Na₂CrO₄ and Cr₂O₃), and Cr(III)- Nano Fe⁰, and Cr(VI)-treated Nano Fe⁰.

sample	Cr concentration	shell	(S ₀ ²) ^a	N	E ₀ (eV)	R (Å)	σ ² (Å ²)	goodness of fit (%)		
Na ₂ CrO ₄ solution	2.0 mM	Cr—O	0.773	4.00	-5.6	1.66	0.0036	4.5		
		Cr ₂ O ₃	66 (%w:w)	Cr—O	0.783	6.00	0.8	1.99	0.0004	6.2
		Cr—Cr ₁	0.783	1.95	0.8	2.93	0.0004			
Cr(III)-nano Fe ⁰	8.0 mmol g ⁻¹	Cr—Cr ₂	0.783	4.00	0.8	3.84	0.0050			
		Cr—O	0.844	6.00	-6.1	1.98	0.0025	5.7		
		Cr—Cr ₁	0.844	1.95	-6.1	3.00	0.0037			
Cr(VI)-nano Fe ⁰	5.2 mmol g ⁻¹	Cr—Cr ₂	0.844	1.00	-6.1	4.03	0.0050			
		Cr—O	0.844	6.00	-6.1	1.97	0.0025	4.9		
		Cr—Cr ₁	0.844	1.95	-6.1	3.05	0.0080			
		Cr—Cr ₂	0.844	1.00	-6.1	3.98	0.0020			

^a The amplitude reduction factor (S₀²) was set at 0.840 during initial fitting and then allowed to vary as a final fitting step; N = coordination number (fixed during the fitting procedure); E₀ = Fermi shift; R = interatomic distance; σ² = Debye-Waller factor; goodness of fit parameter = (Σ(χ_{exp} - χ_{fit})²/Σ(χ_{exp})²) × 100 where χ_{exp} and χ_{fit} are the experimental and calculated χ(k) function data, respectively.

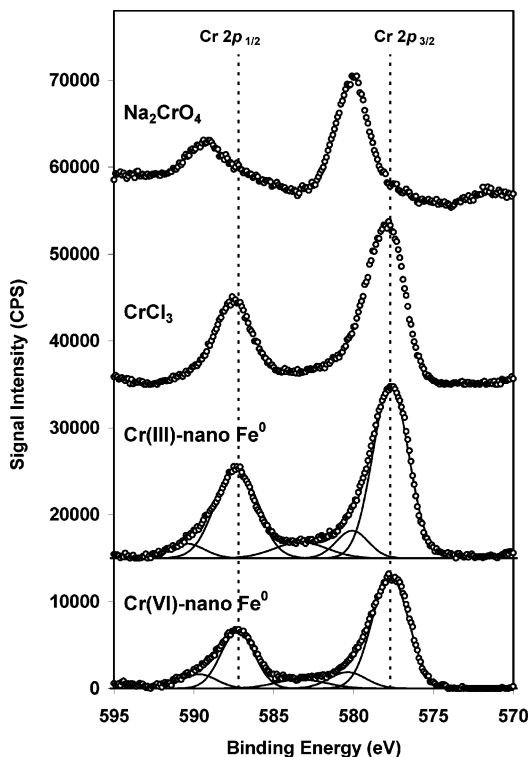


FIGURE 2. Cr 2p line XPS spectra of Na_2CrO_4 , CrCl_3 , and Cr(III)/Cr(VI)-treated nano Fe^0 . Points are experimental data and lines are the results of quantitative Gaussian–Lorentzian curve fitting. Data have been energy corrected using experimental C 1s lines but are not normalized. Vertical dotted lines are the Cr(III) binding energies for Cr $2p_{1/2}$ and Cr $2p_{3/2}$ lines at 587.2 and 577.7 eV, respectively.

12990 correspond closely to the Cr(VI) and Cr(III) solid concentrations of 5.2 and 8.0 mmol g^{-1} nano Fe^0 , respectively, suggesting that the Cr $2p_{3/2}$ peak intensity measurement was operating in a nearly quantitative linear range.

The O 1s line region revealed discrete peak shapes and intensities and was subject to quantitative Gaussian–Lorentzian peak fitting (Figure 3) (see also Table S2 in the Supporting Information). The fitting procedure used structural oxide (O^{2-}) at 530.1 ± 0.2 eV, surface hydroxyl ($-\text{OH}$) at 531.6 ± 0.2 eV, and adsorbed water (H_2O) at 533.2 ± 0.1 eV as components similar to previous investigations (7, 32). Unreacted nano Fe^0 is composed of a $\text{O}^{2-}:-\text{OH}:\text{H}_2\text{O}$ ratio dominated by O^{2-} oxygen. Corrosion of nano Fe^0 particles in 1.0 mM NaCl caused an increase in surface $-\text{OH}$ and a decrease in O^{2-} and the overall peak shape appears similar to synthetic $\gamma\text{-FeOOH}$. These results suggest that corrosion of nano Fe^0 in aqueous solution favors formation of Fe oxyhydroxide polymorphs ($\gamma\text{-FeOOH}$ or $\alpha\text{-FeOOH}$) over Fe oxides such as hematite ($\alpha\text{-Fe}_2\text{O}_3$) or maghemite ($\gamma\text{-Fe}_2\text{O}_3$). Similar O 1s line XPS results were reported for Fe^0 powder treated with Cr(VI)-laden coal fly ash leachate (4, 7).

Nano Fe^0 treatment with Cr(III) and Cr(VI) resulted in increases in the $-\text{OH}:\text{O}^{2-}$ ratio and absolute increases in H_2O (Figure 3). The peak shape is indicative of an aged Cr(OH)₃ material when compared to high-resolution XPS results of Biesenger et al. (32). Final Cr(VI) and Cr(III) solid concentrations after 72 h reaction time were 5.2 and 8.0 mmol g^{-1} nano Fe^0 and yet a greater O 1s signal strength was observed for the Cr(VI)-treated sample than Cr(III)-treated. Despite sample drying, and extensive outgassing during XPS sample introduction, the XPS-accessible surface Cr reaction product in both Cr(VI) and Cr(III) cases is predominantly hydroxylated and hydrous.

XANES Analysis. The analysis of the Fe *K*-edge XANES region of unreacted nano Fe^0 suggested that the bulk particle

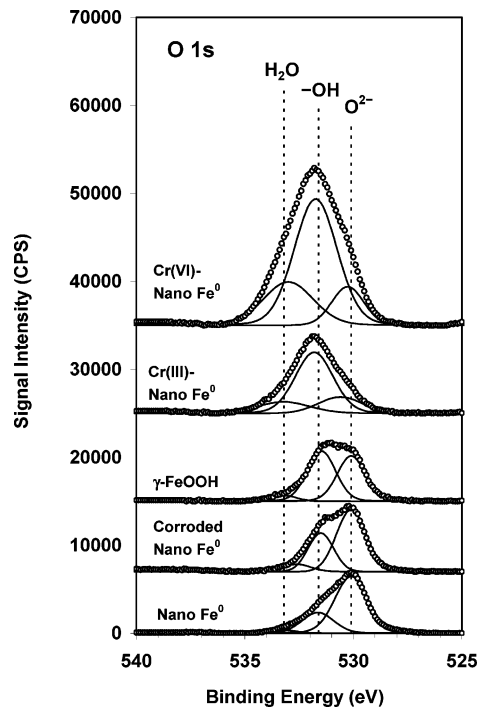


FIGURE 3. O 1s line XPS spectra of unreacted nano Fe^0 , corroded nano Fe^0 , lepidocrocite ($\gamma\text{-FeOOH}$), and Cr(III)/Cr(VI)-treated nano Fe^0 . Points are experimental data and solid lines are the results of quantitative Gaussian–Lorentzian curve fitting showing individual contributions from O^{2-} , $-\text{OH}$, and H_2O . Vertical dotted lines indicate individual O^{2-} , $-\text{OH}$, and H_2O line energies at 530.1 ± 0.2 , 531.6 ± 0.2 , and 533.2 ± 0.2 eV, respectively. Data have been energy corrected using experimental C 1s lines and are not normalized.

Fe oxidation state was metallic Fe^0 when compared with a Fe^0 foil reference (Figure 4a). Corrosion of nano Fe^0 resulted in a positive absorption edge shift of 4 eV when evaluated at mid-height in the spectrum indicative of Fe(III) when compared to model Fe(III) compounds results from previous investigations (41, 42). Normalized Cr *K*-edge XANES results are shown in Figure 4b. The CrO_4^{2-} tetrahedron, which lacks an inversion center, exhibits a preedge peak from a dipole-allowed transition of a 1s electron to an unoccupied antibonding t_2^* tetrahedral orbital. The absence of this feature is evidence of Cr(VI) reduction to lower oxidation state Cr compounds.

The Cr(III)-treated nano Fe^0 was employed in our study as a reference to facilitate analysis of the structure of Cr in the Cr(VI)-treated nano Fe^0 sample without the effects of Cr(VI) reduction. The Cr(III)-treated nano Fe^0 sample is either a Cr(OH)₃ precipitate, $\text{Cr}_x\text{Fe}_{1-x}(\text{OH})_3$ coprecipitate, or possibly a hydrous Cr(III) oxide (CrOOH) since the spectrum does not qualitatively match Cr_2O_3 . The Cr_2O_3 compound has a corundum structure (43) with Cr atoms occupying octahedral sites in the lattice. Octahedral symmetry in XANES spectra is typified by small resonances in the preedge region assigned to transitions of 1s electrons into antibonding orbitals with octahedral symmetry whereas Cr^0 (body centered cubic) shows a broad preedge conduction band feature (44). The XANES analysis of Cr(VI)-treated nano Fe^0 shows that this sample has the same Cr oxidation state and nearly identical Cr electronic environment as Cr(III)-treated nano Fe^0 .

EXAFS Analysis. EXAFS spectroscopy was employed to determine the local atomic structure of Cr in Cr(III)- and Cr(VI)-treated nano Fe^0 . The experimental and fitted Fourier transform results of Cr *K*-edge EXAFS spectra for 2.0 mM Na_2CrO_4 , Cr_2O_3 , and Cr(III)- and Cr(VI)-treated nano Fe^0 are shown in Figure 5 and the fitted values are given in Table 1. Fitting the 2.0 mM Na_2CrO_4 solution data resulted in a shell

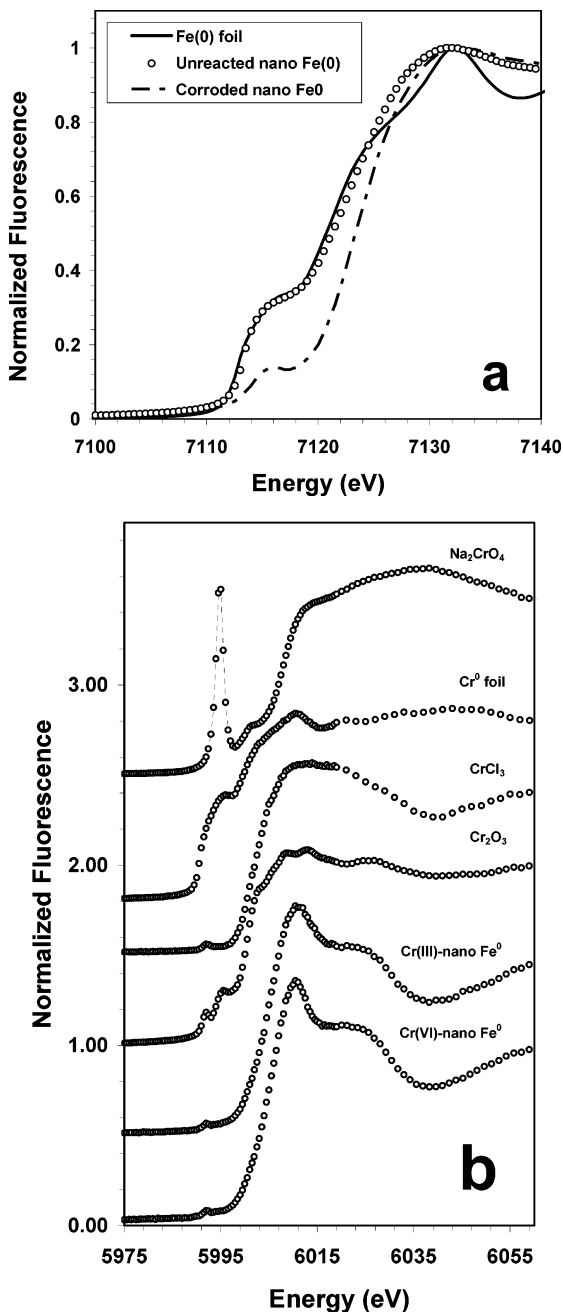


FIGURE 4. K-edge XANES spectra of (a) Fe and (b) Cr samples used in this study. Data have been normalized and offset for clarity.

of $N = 4$ O atoms with a single Cr–O interatomic distance of $R = 1.67 (\pm 0.02)$ Å (Table 1) which is comparable to 1.69 Å reported previously (37). A small second shell peak was noted but not included in the fit. The EXAFS data for Cr(III)- and Cr(VI)-treated nano Fe⁰ (Figure 5) show a coherent Cr–O shell composed of 6 O atoms at distances of 1.98 (± 0.02) and 1.97 (± 0.02) Å, respectively. These distances agree well with a Cr–O distance of 1.99 Å found in previous EXAFS work on synthetic $\text{Cr}(\text{OH})_3 \cdot n\text{H}_2\text{O}$ precipitate (45), Cr(III) adsorption complexes on hydrous Fe(III) oxides (30), and Cr(III) surface precipitates on silica (46). Figure 5 includes Fourier transform results for well-ordered Cr_2O_3 showing features that are distinct from nano Fe⁰ samples. Though the fitted Cr–O distance is comparable ($R = 1.99$ Å), the Cr–O peak has a lower intensity than Cr(III)- and Cr(VI)-treated nano Fe⁰ samples. In addition the Cr_2O_3 sample exhibits a more coherent second shell of Cr atoms at $R = 2.93$ Å.

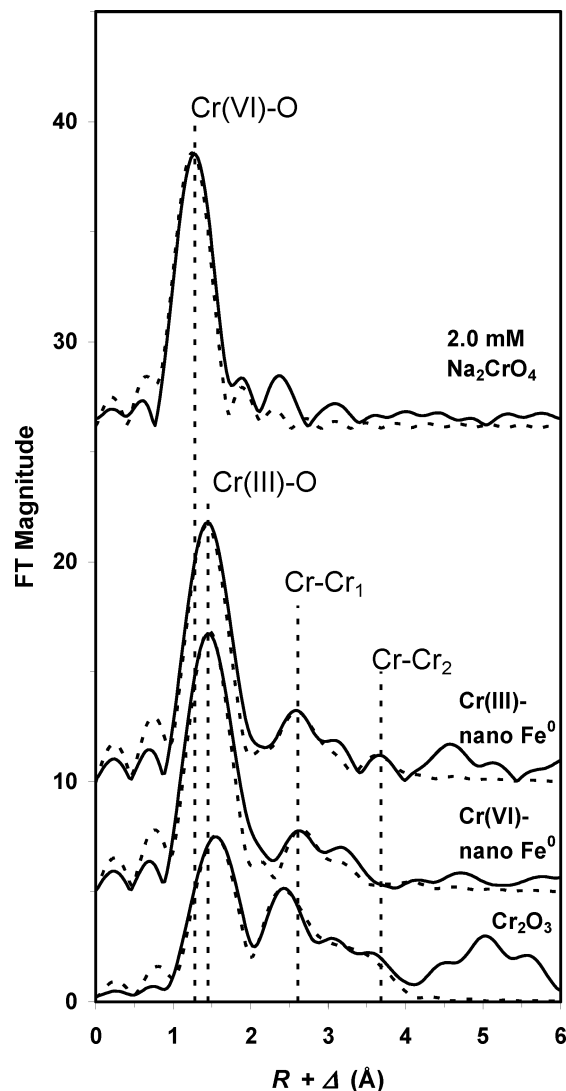


FIGURE 5. EXAFS Fourier transforms of 2.0 mM Na_2CrO_4 solution, Cr(III)- and Cr(VI)-treated nano Fe⁰, and reagent grade Cr_2O_3 (uncorrected for phase shift). Solid lines are experimental data and dotted lines are the fits using SIXPACK software (see numerical results in Table 1).

Fourier transform peaks at distances greater than 1.99 Å were also fit and ascribed to backscattering from Cr–Cr interatomic pairs. In the case of Cr(III)- and Cr(VI)-treated nano Fe⁰, either Cr–Fe or Cr–Cr shells could reasonably be posed in the fit procedure, however EXAFS data analysis cannot discern differences in the atomic number (Z) of nearest neighbors that are $Z \pm 2$ (28) and thus Cr–Cr was used in the present study. Our efforts to model the Cr(III)- and Cr(VI)-treated nano Fe⁰ using Cr–Fe shells gave nearly identical fitted N , R , σ^2 values (data not shown). We found a reasonable fit to our Cr(III)-nano Fe⁰ data using one Cr–O shell at 1.98 Å and two Cr–Cr shells at $R = 3.01 (\pm 0.02)$ Å (Cr–Cr₁) and 4.03 (± 0.02) Å (Cr–Cr₂) interatomic distances (Table 1). The individual contributions of the Cr–O, Cr–Cr₁, and Cr–Cr₂ shells are shown in the Fourier filtered EXAFS data (Figure S4, Supporting Information). The Cr–Cr₁ distance agrees well with previous investigations of Cr(III) surface precipitation on silica (46) and HFO (30). The second Cr–Cr₂ shell fit at $R = 4.03$ Å is close in magnitude to the $R = 3.99$ Å fitted Cr–Cr shell measured in Cr(III)-treated HFO (30).

Previous investigations concluded that Cr(III) adsorption on HFO and goethite occurs via an inner-sphere surface

complexation reaction followed by nucleation and polymerization of Cr(O, OH)₆ polymorphs such as γ -CrOOH (30). In addition, Cr(III) coprecipitated with Fe(III) on HFO was best described as the α -(Cr, Fe)OOH local structure, whereas Cr(III) precipitated alone gave a γ -CrOOH local structure. Due to the similarity between Cr(III)- and Cr(VI)-treated nano Fe⁰ samples, and the overall similarity in appearance of our EXAFS results with previous investigations of Cr(OH)₃·nH₂O formed under various conditions (30, 45–47), it is likely that the product of the reaction of Cr(VI) with nano Fe⁰ is a poorly ordered Cr(OH)₃·nH₂O. However, due to the similarity in chemical properties of the Cr³⁺ and Fe³⁺ ions, and the fact that the techniques used in this study were unable to distinguish between them, it is also possible that Cr_xFe_{1-x}(OH)₃ forms especially under conditions of rapid coprecipitation.

Implications for Remediation of Cr(VI). Though legitimate concerns have been raised about the suitability of nano Fe⁰ for environmental applications due to particle aggregation and stability (38), technological advances such as particle surface modification will eventually overcome these problems and delivering nano Fe⁰ to the contaminated zone in the subsurface will be feasible. The reduction of Cr(VI) to Cr(III) by nano Fe⁰ was shown in this study based on XPS and XANES results. Our results suggest that nano Fe⁰ reduces Cr(VI) and corrodes to form lepidocrocite (a product of Fe(II) oxidation) which then acts as a substrate for precipitation of Cr(OH)₃ and/or Cr_xFe_{1-x}(OH)₃.

Acknowledgments

We thank Matt Newville (APS-GSECARS) for assistance with XAS data collection and Sam Webb (SSRL) for assistance with SIXPACK software work. We also thank Rick Haasch (UIUC Frederick Seitz Materials Research Lab) for assistance with XPS data collection. The EXAFS work was performed at GSECARS (Sector 13, APS), Argonne National Laboratory, which is supported by the NSF (EAR-0217473), the U.S. DOE (DE-FG02-94ER14466), and the State of Illinois. This work was supported by the Research Corporation Cottrell College Science Program (CC6462 and CC5444) and the NSF-MRI program (0421285).

Supporting Information Available

The XRD scan of unreacted nano Fe⁰, C 1s and Fe 2p XPS data, the Fourier filtered EXAFS results, and tables of O 1s and Cr 2p XPS quantitative Gaussian–Lorentzian curve fitting results. This information is available free of charge via the Internet at <http://pubs.acs.org>.

Literature Cited

- Katz, S. A.; Salem, H. *The Biological and Environmental Chemistry of Chromium*; VCH: New York, 1994.
- U.S. EPA. *Field Applications of In Situ Remediation Technology: Permeable reactive Barriers*, EPA 542-R-99-002; U.S. EPA: Washington, DC, 1999.
- Powell, R. M.; Puls, R. W.; Hightower, S. K.; Sabatini, D. A. Coupled iron corrosion and chromate reduction—mechanisms for subsurface remediation. *Environ. Sci. Technol.* **1995**, *29*, 1913–1922.
- Pratt, A. R.; Blowes, D. W.; Ptacek, C. J. Products of chromate reduction on proposed subsurface remediation material. *Environ. Sci. Technol.* **1997**, *31*, 2492–2498.
- Blowes, D. W.; Ptacek, C. J.; Jambor, J. L. In-situ remediation of Cr(VI)-contaminated groundwater using permeable reactive walls: Laboratory studies. *Environ. Sci. Technol.* **1997**, *31*, 3348–3357.
- Puls, R. W.; Paul, C. J.; Powell, R. M. The application of in situ permeable reactive (zerovalent iron) barrier technology for the remediation of chromate-contaminated groundwater: a field test. *Appl. Geochem.* **1999**, *14*, 989–1000.
- Astrup, T.; Stipp, S. L. S.; Christensen, T. H. Immobilization of chromate from coal fly ash leachate using an attenuating barrier containing zero-valent iron. *Environ. Sci. Technol.* **2000**, *34*, 4163–4168.

- Melitas, N.; Chuffe-Moscoco, O.; Farrell, J. Kinetics of soluble chromium removal from contaminated water by zerovalent iron media: Corrosion inhibition and passive oxide effects. *Environ. Sci. Technol.* **2001**, *35*, 3948–3953.
- Gandhi, S.; Oh, B. T.; Schnoor, J. L.; Alvarez, P. J. J. Degradation of TCE, Cr(VI), sulfate, and nitrate mixtures by granular iron in flow-through columns under different microbial conditions. *Water Res.* **2002**, *36*, 1973–1982.
- Wilkin, R. T.; Su, C. M.; Ford, R. G.; Paul, C. J. Chromium-removal processes during groundwater remediation by a zerovalent iron permeable reactive barrier. *Environ. Sci. Technol.* **2005**, *39*, 4599–4605.
- Gu, B.; Phelps, T. J.; Liang, L.; Dickey, M. J.; Roh, Y.; Kinsall, B. L.; Palumbo, A. V.; Jacobs, G. K. Biogeochemical dynamics in zero-valent iron columns: implications for permeable reactive barriers. *Environ. Sci. Technol.* **1999**, *33*, 2170–2177.
- Su, C.; Puls, R. W. Arsenate and arsenite removal by zerovalent iron: Kinetics, redox transformation, and implications for in situ groundwater remediation. *Environ. Sci. Technol.* **2001**, *35*, 1487–1492.
- Furukawa, Y.; Kim, J.-w.; Watkins, J.; Wilkin, R. T. Formation of ferrihydrite and associated iron corrosion products in permeable reactive barriers of zero-valent iron. *Environ. Sci. Technol.* **2002**, *36*, 5469–5475.
- Manning, B. A.; Hunt, M.; Amrhein, C.; Yarmoff, J. A. Arsenic(III) and arsenic(V) reactions with zerovalent iron corrosion products. *Environ. Sci. Technol.* **2002**, *36*, 5455–5461.
- Eary, L. E.; Rai, D. Chromate removal from aqueous wastes by reduction with ferrous ion. *Environ. Sci. Technol.* **1988**, *22*, 972–977.
- Li, Z.; Jones, H. K.; Bowman, R. S.; Helferich, R. Enhanced reduction of chromate and PCE by palletized surfactant-modified zeolite/zerovalent iron. *Environ. Sci. Technol.* **1999**, *33*, 1291–1298.
- Ponder, S. M.; Darab, J. G.; Mallouk, T. E. Remediation of Cr(VI) and Pb(II) aqueous solutions using supported, nanoscale zero-valent iron. *Environ. Sci. Technol.* **2000**, *34*, 2564–2569.
- Anderson, L. D.; Kent, D. B.; Davis, J. A. Batch experiments characterizing the reduction of chromium(VI) using suboxic material from a mildly reducing sand and gravel aquifer. *Environ. Sci. Technol.* **1994**, *28*, 178–185.
- Fendorf, S.; Li, G. Kinetics of chromate reduction by ferrous iron. *Environ. Sci. Technol.* **1996**, *30*, 1614–1617.
- Sedlak, D. L.; Chan, P. G. Reduction of hexavalent chromium by ferrous ions. *Geochim. Cosmochim. Acta* **1997**, *61*, 2185–2192.
- Buerge, I. J.; Hug, S. J. Kinetics and pH dependence of chromium(VI) reduction by iron(II). *Environ. Sci. Technol.* **1997**, *31*, 1426–1432.
- Buerge, I. J.; Hug, S. J. Influence of mineral surfaces on Cr(VI) reduction by iron(II). *Environ. Sci. Technol.* **1999**, *33*, 4285–4291.
- Liu, Y.; Choi, H.; Dionysiou, D.; Lowry, G. V. Trichloroethene hydrodechlorination in water by highly disordered monometallic nanoiron. *Chem. Mater.* **2005**, *17*, 5315–5322.
- Liu, Y.; Majetich, S. A.; Tilton, R. D.; Sholl, D. S.; Lowry, G. V. TCE dechlorination rates, pathways, and efficiency of nanoscale iron particles with different properties. *Environ. Sci. Technol.* **2005**, *39*, 1338–1345.
- Wang, C. B.; Zhang, W. Synthesizing nanoscale iron particles for rapid and complete dechlorination of TCE and PCBs. *Environ. Sci. Technol.* **1997**, *31*, 2154–2156.
- Kanel, S. R.; Manning, B. A.; Charlet, L.; Choi, H. Removal of arsenic(III) from groundwater by nano-scale zero-valent iron. *Environ. Sci. Technol.* **2005**, *39*, 1291–1298.
- Ponder, S. M.; Darab, J. G.; Bucher, J.; Caulder, D.; Craig, I.; Davis, L.; Edelstein, N.; Lukens, W.; Nitsche, H.; Rao, L.; Shuh, D. K.; Mallouk, T. E. Surface chemistry and electrochemistry of supported zerovalent iron nanoparticles in the remediation of aqueous metal contaminants. *Chem. Mater.* **2001**, *13*, 479–486.
- Patterson, M. L.; White, A. F.; Brown, G. E., Jr.; Parks, G. A. Surface passivation of magnetite by reaction with aqueous Cr(VI). *Environ. Sci. Technol.* **1997**, *31*, 1573–1576.
- Davis, A.; Olsen, R. L. The Geochemistry of chromium migration and remediation in the subsurface. *Ground Water* **1995**, *33*, 759–768.
- Charlet, L.; Manceau, A. A. X-ray absorption spectroscopic study of the sorption of Cr(III) at the oxide-water interface: II. Adsorption, coprecipitation, and surface precipitation on hydrous ferric oxide. *J. Colloid Interface Sci.* **1992**, *148*, 443–458.

- (31) Schwertmann, U.; Cornell, R. M. *Iron oxides in the laboratory: Preparation and characterization*; VCH: New York, 1991; pp 81–83.
- (32) Biesinger, M. C.; Brown, C.; Mycroft, J. R.; Davidson, R. D.; McIntyre, N. S. X-ray photoelectron spectroscopy studies of chromium compounds. *Surf. Interface Anal.* **2004**, *36*, 1550–1563.
- (33) Burrell, M. C.; Chera, J. J. Charge correction of the binding energy scale in XPS analysis of polymers using surface deposition of PDMS. *Surf. Interface Anal.* **1999**, *27*, 811–815.
- (34) Webb, S. M. SIXPACK: A graphical user interface for XAS analysis using IFEFFIT. *Phys. Scr.* **2005**, *T115*, 1011–1014.
- (35) Newville, M. IFEFFIT: interactive XAFS analysis and FEFF fitting. *J. Synchrotron Rad.* **2001**, *8*, 324–332.
- (36) Rehr, J. J.; Zabinsky, S. I.; Albers, R. C. High-order multiple-scattering calculations of X-ray absorption fine structure. *Phys. Rev. Lett.* **1992**, *69*, 3397–3400.
- (37) Fendorf, S. E.; Eick, M. J.; Grossl, P.; Sparks, D. L. Arsenate and chromate retention mechanisms on goethite. 1. Surface structure. *Environ. Sci. Technol.* **1997**, *31*, 315–320.
- (38) Nurmi, J. T.; Tratnyek, P. G.; Sarathy, V.; Baer, D. R.; Amonette, J. E.; Pecher, K.; Wang, C.; Linehan, J. C.; Matson, D. W.; Penn, R. L.; Driessen, M. D. Characterization and properties of metallic iron nanoparticles: Spectroscopy, electrochemistry, and kinetics. *Environ. Sci. Technol.* **2005**, *39*, 1221–1230.
- (39) Qiu, S. R.; Lai, H.-F.; Roberson, M. J.; Hunt, M. L.; Amrhein, C.; Giancarlo, L. C.; Flynn, G. W.; Yarmoff, J. A. Removal of contaminants from aqueous solution by reaction with iron surfaces. *Langmuir* **2000**, *16*, 2230–2236.
- (40) Qin, F.; Magtoto, N. P.; Garza, M.; Kelber, J. A. Oxide film growth on Fe(111) and scanning tunneling microscopy induced high electric field stress in Fe₂O₃/Fe(111). *Thin Solid Films* **2003**, *444*, 179–188.
- (41) Wilke, M.; Farges, F.; Petit, P. E.; Brown, G. E., Jr.; Martin, F. Oxidation state and coordination of Fe in minerals: An Fe K-XANES spectroscopic study. *Am. Mineral.* **2001**, *86*, 714–730.
- (42) O'Day, P. A.; Rivera, N., Jr.; Root, N. R.; Carroll, S. A. X-ray absorption spectroscopic study of Fe reference compounds for the analysis of natural sediments. *Am. Mineral.* **2004**, *89*, 572–585.
- (43) Rosso, K. M.; Rustad, J. R. Structures and energies of AlOOH and FeOOH polymorphs from plane wave pseudopotential calculations. *Am. Mineral.* **2001**, *86*, 312–317.
- (44) Arçon, I.; Mirtič, B.; Kodre, A. Determination of valence states of chromium in calcium chromates by using X-ray absorption near-edge structure (XANES) spectroscopy. *J. Am. Ceram. Soc.* **1998**, *81*, 222–224.
- (45) Manceau, A. A.; Charlet, L. X-ray absorption spectroscopic study of the sorption of Cr(III) at the oxide-water interface : I. Molecular mechanism of Cr(III) oxidation on Mn oxides. *J. Colloid Interface Sci.* **1992**, *148*, 425–442.
- (46) Fendorf, S. E.; Lamble, G. M.; Stapleton, M. G.; Kelley, M. J.; Sparks, D. L. Mechanisms of chromium(III) sorption on silica. 1. Cr(III) surface structure derived by extended x-ray absorption fine structure spectroscopy. *Environ. Sci. Technol.* **1994**, *28*, 204–289.
- (47) Laget, V.; Jeffcoate, C. S.; Isaacs, H. S.; Buchheita, R. G. Dehydration-induced loss of corrosion protection properties in chromate conversion coatings on aluminum alloy 2024-T3. *J. Electrochem. Soc.* **2003**, *150*, B425–B432.

Received for review July 20, 2006. Revised manuscript received October 24, 2006. Accepted October 25, 2006.

ES061721M